

# Directing Chemotaxis-Based Spatial Self-Organization via Biased, Random Initial Conditions

Sean Grimes, Linge Bai, Andrew W.E. McDonald, and David E. Breen\*

{spg63,lb353,awm32,david}@cs.drexel.edu  
+1 215-895-2669

Department of Computer Science  
Drexel University  
3141 Chestnut Street  
Philadelphia, PA 19104  
USA

This research was funded by National Science Foundation grants CCF-0636323  
and IIS-0845415.

\* Corresponding author.

arXiv:1803.03654v1 [cs.MA] 9 Mar 2018

*The International Journal of Parallel, Emergent and Distributed Systems*  
Vol. 00, No. 00, Month 2011, 2–31

## RESEARCH ARTICLE

# Directing Chemotaxis-Based Spatial Self-Organization via Biased, Random Initial Conditions

Sean Grimes, Linge Bai, Andrew W.E. McDonald, and David E. Breen\*

*Department of Computer Science, Drexel University Philadelphia, PA 19104 USA*

*(Received 00 Month 200x; in final form 00 Month 200x)*

Inspired by the chemotaxis interaction of living cells, we have developed an agent-based approach for self-organizing shape formation. Since all our simulations begin with a different uniform random configuration and our agents move stochastically, it has been observed that the self-organization process may form two or more stable final configurations. These differing configurations may be characterized via statistical moments of the agents' locations. In order to direct the agents to robustly form one specific configuration, we generate biased initial conditions whose statistical moments are related to moments of the desired configuration. With this approach, we are able to successfully direct the aggregating swarms to produced a desired macroscopic shape, starting from randomized initial conditions with controlled statistical properties.

**Keywords:** spatial self-organization, directed emergence, genetic programming, agent-based system, statistical moments

## 1. Introduction

Motivated by the ability of cells to form into specific shapes and structures, in previous work we developed chemotaxis-inspired software agents for self-organizing shape formation [1, 2]. The actions of the agents, which we call Morphogenetic Primitives (MPs), are based on the behaviors exhibited by living cells. Cells emit chemicals into the environment. Neighboring cells detect the overall chemical concentration at their surfaces and respond to the chemical stimulus by moving along the chemical field's gradients [3]. Similarly, in our system the agents emit a virtual chemical, with its concentration defined by an explicit mathematical expression. A set of agents start with an initial random configuration and stochastically follow the gradient of the cumulative concentration field. These chemotaxis-based local interactions direct the agents to self-organize into user-specified shapes (Figure 1). Since the behaviors of MPs are based on local information and interactions, they could provide a distributed, scalable approach for controlling the movements of a robotic swarm.

---

\*Corresponding author. Email: david@cs.drexel.edu, +1 (215) 895-1626

In some cases, we have observed though that the agents do not spatially self-organize into a unique shape, but instead form two or more stable final configurations. If MPs are used to control the motions of individual robots, it would be extremely useful to direct the outcome of these bifurcating spatial self-organization processes towards a consistent outcome. This would allow us to guarantee that all of our MP aggregations produce a single, desired shape. This is a property that is essential for robust and predictable swarm control algorithms, one that would make the algorithm reliable for engineering applications. Towards this end, we have analyzed whole swarm populations at a global level in search of macroscopic, distinguishing attributes. This analysis identified features, based on statistical moments of the agents' positions, that have significantly different values for different outcomes of a swarm aggregation. In earlier work we discovered that these statistical moments can be used to accurately predict the outcome of the self-organization process at an early stage of the shape aggregation [4]. Given these differentiating moments, the work described here investigated techniques for directing the outcome of our self-organizing system via biased, random initial conditions in order to consistently produce a desired final configuration.

Through our study of the dynamics of a swarm's statistical moments during the aggregation process we noted the connection between initial conditions and the final shape configuration of the swarm. We discovered that biased, random initial conditions that meet specified constraints, i.e. have well-defined statistical properties, robustly yield simulations with a unique final outcome. For those agent interactions that ultimately produce bifurcating/multiple shapes, we have identified for each shape, the most distinguishing macroscopic statistical moment of the evolving swarm. It is possible to generate random distributions of MPs that have specific statistical moments. Our work empirically shows that for bifurcating self-organizing, non-linear, dynamical systems (e.g. a swarm of Morphogenetic Primitives) one final outcome can be consistently generated by enforcing a constraint on the value of a single moment when generating the swarm's initial conditions. Given this feature of our system, we are able to control the final outcome of the simulation by simply thresholding the value of a statistical moment for a particular starting distribution, i.e., we constrain the random initial conditions to have specific statistical properties.

## 2. Related Work

Research on distributed agent-based systems that can form spatial patterns and shapes, as well as swarm behaviors, has been conducted for several decades. Reynolds [5] proposed the seminal model for simulating flocking and schooling behaviors based on the local interactions of "boids". Fleischer and Barr [6, 7] explored a cell-based developmental model for self-organizing geometric structures. Theraulaz and Bonabeau [8, 9] presented a modeling approach based on the swarming behavior of social insects. They combined swarm techniques with 3D cellular automata to create autonomous agents that indirectly interact in order to create complex 3D structures. Viscek et al. [10] investigated a particle-based model related to the Reynolds model and found that macroscopic phase changes occurred

in the particle system when introducing noise in the local interactions. Jadbabaie et al. [11] further explored the Vicsek model and provided a theoretical explanation for the model's observed behavior, as well as convergence results for classes of switching signals and arbitrary initial heading vectors.

The initial work in this area of research created distributed, locally-interacting agent-based systems, then observed and characterized their behaviors. Later work explored techniques for directing these distributed, self-organizing systems. Eggenberger Hotz [12, 13] proposed the use of genetic regulatory networks coupled with developmental processes for use in artificial evolution and was able to evolve simple shapes. Bonabeau et al. [14] applied genetic algorithms to the stigmergic swarm-based 3D construction method of Theraulaz and Bonabeau in order to evolve interactions that produce user-acceptable structures. Nagpal et al. [15, 16] presented techniques to achieve programmable self-assembly. Cells are identically-programmed units which are randomly distributed and communicate with each other within a local area. In this approach, global-to-local compilation is used to generate the program executed by each cell, which has specialized initial parameters. Stoy and Nagpal [17] presented an approach to self-reconfiguration based on directed growth, where the desired configuration (which is stored in each module) is grown from an initial seed module. Spare modules move along recruitment gradients emanating from attached modules to create the final shape. Gradients derived from global potential fields have also been investigated for directing robot swarms. Both Rimon and Koditschek [18] and Hsieh and Kumar [19] demonstrated that robot paths and controls can be computed from these fields, which lead the robots to form a pre-defined shape.

Shen et al. [20] proposed a Digital Hormone Model for directing robot swarms to perform such tasks as surrounding a target, covering an area and bypassing barriers. The model relies on local communications between identical agents, but it also has each agent move towards a single global target. Swarm chemistry, proposed by Sayama [21, 22] and based on Reynolds' model, is an approach for designing spatio-temporal patterns for kinetically interacting, heterogeneous agents. An interactive evolutionary method, similar to Sims' [23], has been used to define system parameters that lead to agent segregation and structure formation. Mamei et al. [24] proposed a distributed algorithm for robots that are attracted to and aggregate around targets sensed over short distances. By electing leader(s) as barycenter(s), propagating gradients of varying structure and using these gradients as instruction conditionals, a swarm of simulated robots are able to self-organize into a number of simple shapes such as a circle, ring, and lobes. Von Mammen and Christian [25] described swarm grammars, an agent-based extension of Lindenmayer systems, that are capable of adapting to their environment and evolve agent parameters in order to create structures that incorporate aspects of developmental design and morphogenesis. The field of Guided Self-Organization (GSO) [26] has developed techniques for steering self-organizing systems towards desired outcomes, while still attempting to not constrain the system's configuration space during its evolution.

Doursat [27, 28] proposed a model for artificial development which combines proliferation, differentiation, self-assembly, pattern formation and genetic regulation. Via genetic-like regulation at the agent level, the agents can self-organize into a number of patterned shapes and structures. Werfel et al. [29] proposed a de-

centralized multi-agent system approach, inspired by mound-building termites, for building user-defined structures. A user specifies a desired structure, and the system automatically generates low-level rules for independent climbing robots that guarantee production of the structure. A single “seed” brick is used as a landmark to identify where the structure is going to be built, and defines the origin of a shared coordinate system for the robots. Gerling and Von Mammen [30] provided a context for this type of work in a summary of self-organized approaches to construction.

Our previous and latest work on agent-based shape formation stands apart from related work in that it utilizes a chemotaxis-based interaction paradigm inspired by the behaviors of living cells which leads to the formation of tissues. Given the goal of recreating the properties of cells, MPs were designed with principles that should make them scalable and robust [2]. These design principles define MPs as identical, distributed agents that are not directed by a ‘master designer’, exchange information locally, carry no representation of the shape to be formed, and have no information about their global location. The macroscopic shape of the swarm emerges from the aggregation of local interactions and behaviors. Our approach is therefore novel compared to previous work in that it contains all of the following features. 1) All morphogenetic primitives are randomly placed in the environment, are identical, and perform the same simple actions, unlike Nagpal et al. [15, 16]), Mamei et al. [24], and Doursat [27, 28]. They require no differentiated behaviors or customized initialized states. 2) No initialization of spatial information is needed in the computational environment, unlike Stoy and Nagpal [17], Shen et al. [20], and Werfel et al. [29]. 3) Individual MPs do not know their location in any external/global coordinate system, unlike Stoy and Nagpal [17], and [29]. 4) MPs do not contain or utilize a representation of the predefined global shape that is being composed, unlike Stoy and Nagpal [17], Rimon and Koditschek [18], and Hsieh and Kumar [19]. 5) We utilize genetic programming to discover the MP concentration field functions that lead to the formation of a user-specified shape. Chemotaxis then provides a straightforward mechanism for determining the motion of MPs, in contrast to the difficult-to-program approaches of Shen et al. [20] and Sayama [21, 22]. Note that our new work described here enhances our previously developed system [2] to make MPs more robust, consistent and reliable.

### **3. Background Material**

#### ***3.1 Agent-based Shape Formation***

Like Pfeifer et al. [31] we turn to biology and self-organization for insights into the design of autonomous robots, robotic swarms in our case. Our previous work in self-organizing shape formation [2, 32] is inspired by developmental biology [33] and morphogenesis [34], and builds upon a chemotaxis-based cell aggregation simulation system [35]. Morphogenesis is the process that forms the shape or structure of an organism through cell shape change, movement, attachment, growth and death. We have explored chemotaxis as a paradigm for agent system control because the motions induced by chemotaxis (one of the mechanisms of morphogenesis) may produce patterns, structures or sorting of cells [36].

### 3.1.1 Morphogenetic Primitives

Morphogenetic Primitives are initially placed inside a  $2D$  environment with a random uniform distribution. Each MP is represented by a small disc and emits a ‘chemical’ into the environment within a fixed distance relative to its own local coordinate system. Every MP emits the identical local chemical field. An MP detects the cumulative chemical field at eight receptors on its surface, and calculates the field gradient from this input. MPs move in the direction of the field gradient with a speed proportional to the magnitude of the gradient. By employing these relatively simple chemotaxis-inspired behaviors MPs are able to self-organize into user-specified macroscopic shapes.

This process is schematically presented in the bottom 2/3 of Figure 2. In the middle left of the figure, a close-up of an MP is provided showing its eight chemical sensors and the range of the finite chemical field that it emits. Numerous MPs are randomly placed in the computational arena, and are provided as initial conditions to a chemotaxis-based cell aggregation simulator. The simulator then computes an aggregation simulation based on the one chemical field that is associated with all MPs. The self-organization of the agent swarm is shown in the middle right of the figure. The bottom flowchart of the figure outlines the steps taken by the cell simulator for each cell. The bottom left image shows a representative MP chemical field, with the chemical concentration visualized with gray-scale colors. Isolines are added to highlight the structure of the chemical field. The image to its right shows a cumulative chemical field given the contributions of all of the MPs in the arena. The top part of the figure will be explained later in the paper.

### 3.1.2 Genetic Programming for Discovering Local Interactions

While MPs’ fundamental interactions are based on a chemotaxis-inspired paradigm, we do not limit their behaviors/properties to be physically realistic or completely consistent with biology. Instead, developmental biology provides a motivating starting point for MPs. As a way to customize chemotaxis-inspired agents for shape formation, we alter the chemical concentration fields around individual cells. Instead of the chemical concentration dropping off only as an inverse function of distance  $d$  from the cell’s surface (e.g.  $1/d$ ), in our system we define the concentration field with an explicit function of  $d$  and  $\theta$ , the angular location in the cell’s local coordinate system.

Currently, there is no prescriptive way to specify a particular local field function that will direct MPs to form a specific macroscopic shape, we therefore employ genetic programming [37] to produce the mathematical expression that explicitly specifies the field function. In order to meet the substantial computational requirement imposed by our evolutionary computing approach, we have implemented a master-slave form of the distributed genetic programming process [1]. The fitness measure associated with each individual field function is based on the shape that emerges from the chemical-field-driven aggregation simulation, and determines which functions will be passed along to later generations. The genetic process stops once an individual (i.e., a mathematical expression) in the population produces the desired shape via a chemotaxis simulation, or after a certain number of generations have been produced and evaluated. Figure 3 illustrates this approach. See [1], [2] and [38] for more details on MPs and the software system that implements them.

With this algorithm, we have successfully evolved local MP chemical field functions for a number of simple shapes [2]. These results support the proposition that biological phenomena offer paradigms for designing cellular primitives for self-organizing shape formation. While the resulting explicit chemical fields are not biologically/chemically plausible, they do provide an approach for controlling robot swarms that communicate wirelessly over short distances and share minimal information with each other. Thus the agents in the swarm do not require significant compute power to self-organize. Additionally, evolutionary computing techniques, specifically genetic programming, have been crucial for discovering the detailed local interactions that lead to the emergence of the swarm's macroscopic structure.

However, given the MPs' initial random configurations and the stochastic nature of the self-organization process, the outcomes of the simulations with a specific field function are not always the same. We have found that the shape formation simulations, which include random displacements of the MPs and noise in their movements, can generate bifurcating results. For some field functions, if we run numerous simulations each starting with a different random uniform distribution of MPs, two sets of final configurations will be formed. In most cases an equal number of each configuration are produced, but in a few cases the ratio of the numbers is not one. Since it would be useful to control the outcomes of the self-organization process, we have developed methods for directing the final configuration of a bifurcating simulation by starting the simulation with biased initial conditions [39].

### 3.2 Outcome Prediction

The first step towards developing methods that direct the outcome of a swarm simulation involved identifying spatial features that are correlated with and can differentiate the final, different swarm configurations. Our initial effort towards achieving this goal investigated methods for predicting the final configuration of a bifurcating simulation at an early stage of the aggregation process. Our reasoning was that if certain spatial features can be used to predict the outcome of an aggregation, then they represent unique attributes of the swarm that could be manipulated to direct the swarm. In order to predict the final outcome of a self-organizing shape formation simulation, we first extracted features that capture the spatial distribution of the MPs. Moments provide a quantitative way to describe a distribution. Since MPs are defined as small discs, we use the center of each disc to represent each MP's location. We therefore can simplify the collection of MP locations as a set of  $2D$  points, and apply moment analysis to this set over the duration of the MP simulation.

We calculated the mean (first moment), variance (second central moment), skewness (third central moment) and kurtosis (fourth central moment) from the  $x$  and  $y$  coordinates of the MP centers. We analyzed the locations  $X_i$  of all points (MPs) as a whole, rather than tracking the location and movement of each individual point. The population size of the agents is denoted as  $n$ , ( $n = 500$ ), and the formulas of

the four moments  $M_1$  to  $M_4$  are given in Equations 1 to 4,

$$M_1 = \frac{1}{n} \sum_{i=1}^n X_i, \quad (1)$$

$$M_2 = \frac{1}{n} \sum_{i=1}^n (X_i - M_1)^2, \quad (2)$$

$$M_3 = \left[ \frac{1}{n} \sum_{i=1}^n (X_i - M_1)^3 \right] / (M_2)^{3/2}, \quad (3)$$

$$M_4 = \left[ \frac{1}{n} \sum_{i=1}^n (X_i - M_1)^4 \right] / (M_2)^2. \quad (4)$$

These statistical moments provide quantitative information about the shape of histograms/distributions. When computed for the  $x$  and  $y$  coordinates of the MPs, these moments capture the asymmetry and shape of the spatial distribution of the whole population. We have not found it necessary to compute cross moments, with the first four moments providing sufficient information for our analysis. Since the  $x$  and  $y$  coordinates of the points change over time, so do the four moments of the distribution of the  $x$  and  $y$  values. The change of the moments as a function of simulation time also provides insight into the dynamic nature of a particular MP simulation.

At each simulation time  $t$ , the four moments  $M_i(t)$  ( $i = 1$  to  $4$ ) of the overall distribution are calculated. We then approximate the time derivative of the moments as the slope of a linear interpolating function of consecutive moment values. By calculating the moments and their time derivatives for both the  $x$  and  $y$  coordinates of the point set, at a given time  $t$ , we obtain a 16-dimensional vector to represent the distribution,

$$M_{x_1}(t), M_{y_1}(t), M_{x_2}(t), M_{y_2}(t), M_{x_3}(t), M_{y_3}(t), M_{x_4}(t), M_{y_4}(t), k_{x_1}(t), k_{y_1}(t),$$

$$k_{x_2}(t), k_{y_2}(t), k_{x_3}(t), k_{y_3}(t), k_{x_4}(t), k_{y_4}(t).$$

Given the sensitivity of non-linear dynamical systems to initial conditions [40], it makes it extremely difficult, if not impossible, to predict the outcome of our complex, self-organizing system from its initial, random spatial configuration. We therefore attempted to predict the final spatial configuration at an early stage of the aggregation, usually before it is visually evident what shape will emerge from the process. We considered prediction of the bifurcating outcomes as a classification problem and utilized support vector machines (SVMs) [41] to solve it. We have found that applying SVMs to the distribution feature vector at a simulation time that is a small percentage of the total time needed for the final aggregated shape to form produced acceptable results. Given 200 MP simulations for a variety of bifurcating self-organizing shapes we found that we could predict the outcome of the aggregation at a time point 5% to 10% into the simulation with an accuracy of 81% to 91%. We view these results as satisfactory because they demonstrate that a strong correlation between a swarm's moments and its final formed shape does



exist. More details about this study may be found in [39] and [4].

#### 4. Directing Spatial Self-Organization

Since the outcome of an MP simulation can be predicted at an early stage of aggregation using the moments of the agents' positions, we then explored methods for controlling the swarm via manipulating the moments of the swarm's initial configuration. The general strategy is to create random initial configurations for the MP simulations, but with constrained, biased moments. We have observed that this strategy can consistently direct the swarm to aggregate into specific final configurations. The first step of the strategy analyzes the bifurcating simulations to determine which of the moments diverge the most for the two different outcomes. This is the moment that will be biased in the swarm's initial, random configuration.

##### 4.1 Moment Analysis

One of our aggregations, which produces what we call the quarter-moon shape, provides an example of the moment analysis. Of the 200 simulations starting with a uniform random, unbiased initial condition, 100 produce left-pointing structures and 100 produce right-pointing structures. Figure 5 shows a typical swarm aggregation for this shape. The four moments of both  $x$  and  $y$  coordinates are calculated over all 35,000 simulation steps. Additionally the mean and standard deviation of each statistical moment are calculated for the two categories, i.e. left-pointing and right-pointing, over the simulation time steps. Plotting the mean and the mean  $\pm$  standard deviation of the moments over time immediately highlights the moments which are the most differentiating and may be used to identify specific shapes. For the quarter-moon example the third  $x$  moment (skewness) is the one with the greatest separation of values for the two possible outcomes, as seen in Figure 6. The solid and dashed lines are the mean of the skewness of the  $x$  coordinate for the two outcomes. The dotted and dot-dashed lines are mean  $\pm$  standard deviation. The dashed curve is produced from structures that are right-pointing and follow the path in the top of Figure 5. The solid curve is produced from the left-pointing structures, with a typical aggregation presented at the bottom of Figure 5.

By analyzing the time series in Figure 6, we see that the skewness of the  $x$  coordinates of the two classes starts at about the same value, approximately  $-0.05$  to  $0.05$ , at time step 0. The values should be near zero, since all simulations begin with uniform random configurations. The skewness of the two classes first separates by increasing or decreasing, followed by a zero crossing and then a reversed trend appears until they reach their final states at step 35,000. Observing the values for the solid and dashed curves over all simulation time steps, we can identify three regions in the plot: a region occupied by solid/dotted curves only, a region occupied by dashed/dot-dashed curves only and an overlapping region. To be specific, considering the values of  $x$  skewness in Figure 6 (by projecting the curves into the  $y$  axis), the range of  $[-0.195, -0.150]$  is covered by solid/dotted curves only;  $[0.150, 0.190]$  is covered by dashed/dot-dashed curves only and  $[-0.150, 0.150]$  is covered by both outcomes.

When determining the appropriate threshold value for a constrained moment, we start with the mean value of the non-overlapping moment range for a particular shape, and then adjust if needed. For the region covered only by the quarter-moon's dashed/dot-dashed curves (for right-pointing shapes) the mean value of skewness is 0.170. While using this value for the moment constraint produced reasonable results (94% of the biased initial conditions produced the desired shape), we found, via multiple experimental runs, that the threshold value on the skewness had to be increased to produce a consistent result. In general this was the process employed for determining the moment constraint thresholds needed to generate the desired outcomes.

#### 4.2 Generating Constrained Biased Distributions

Once the most significant distinguishing moment (the one with the greatest value difference in the final configuration) for a shape is identified, the information is utilized to direct the shape aggregation by imposing constraints on this moment in the initial conditions. We assume that the MPs'  $x$  and  $y$  coordinates are independent, and therefore create two probability density functions, each representing the  $x$  and  $y$  coordinate. One probability density function is created for the constrained coordinate and the other coordinate is considered to be uniformly random. Samples are drawn independently from the two distributions to produce a single  $(x, y)$  location.

This approach generates random distributions, i.e. 2D random initial configurations for the shape simulation, that meet a constraint on a particular moment in the  $x$  or  $y$  coordinate. We have found that constraining one of the eight moments (mean, variance, skewness and kurtosis for  $x$  and  $y$ ) is sufficient for producing satisfactory results. Constraining multiple moments does not significantly improve the outcomes, and would further complicate the process of generating initial conditions. Once one significant moment of a distribution and its threshold value have been identified, the remaining three moments for that spatial coordinate ( $x$  or  $y$ ) may be set to values observed in uniform random distributions. These values are *mean* = 500 (the center of our computational arena), *variance* = 15,000, *skewness* = 0 (to make the distribution symmetric), and *kurtosis* = 2. Once the four moments for one of the coordinates have been specified, a probability density function (PDF) with those moments is defined. The values for the other coordinate are generated from a uniform random distribution.

For the constrained dimension we create a Gram-Charlier expansion of the normal distribution (chosen for its convergence properties) with specified moments [42]. This Gaussian-expanded probability density function is then discretized with 100,000 samples with values falling within the range of 0 to 1000 (the range of the computational arena). Slice sampling [43], a Markov chain sampling method chosen for its efficiency, is then utilized to draw 500 samples from this discretized distribution. Theoretically, the specified PDF can be sampled to produce a distribution that has the same moments as the PDF. Our experience has shown that the sample size needs to be quite large (on the order of 1 million) for this to be true. For our sample size of 500 (the number of MPs in an aggregation simulation) and heavily biased PDFs, the resulting moments of the finite sample set do not

necessarily match the ones desired for a particular shape.

As the distribution generation process cannot guarantee that a sampled distribution will meet the required moment constraints, the four moments of the generated distributions for the constrained coordinate are computed to determine if the constraint is actually met. If the value of the significant moment is not above or below (depending on the constraint to be enforced) the specified threshold, the sampled distribution is rejected. If the constraint is met, the distribution is accepted as the initial conditions for a simulation computation.

Since our agents are not points, but in fact are discs with a fixed radius, we maintain a distance of  $2R$  (where  $R$  is the radius of a disc) between sample points, to ensure that the MPs do not overlap. Therefore, if an  $(x, y)$  pair is generated that is less than  $2R$  distance to a previously generated location, it is rejected and another  $(x, y)$  pair is calculated. This process continues until a sufficient number of MP locations are generated for the initial conditions.

We have found that it is more computationally efficient to generate numerous smaller sample sets and then merge them into a single point set, rather than attempt to compute a single, large point sample, when composing biased initial conditions for our aggregation simulations. We apply this approach by drawing 50 subsets,  $T_{k=1, \dots, 50}$  of 10 samples, rather than 1 set of 500 samples. Each sample drawn is checked for overlap with existing samples, discarded if overlap exists, and otherwise added to the current  $T_k$ . Once each  $T_k$  has 10 samples, it is checked for conformance to the moment restrictions prior to insertion into the final set,  $S$ , of 500 samples. If a given  $T_k$  fails, a new  $T_k$  is drawn. An acceptable  $T_k$  is merged with  $S$ , which is then checked for conformance to the moment restrictions. If the updated  $S$  does not pass, it is reverted to its prior state,  $S - T_k$ , and a new  $T_k$  is drawn. This process continues until  $|S| = 500$ . The algorithm for generating biased initial condition, once the initial sampling does not meet the moment requirements, is diagrammed in the flowchart at the top of Figure 2. Via this approach, we are able to generate initial conditions for our computational experiments in a few seconds, as opposed to several hours, when attempting to generate all 500 points of  $S$  at once for certain “extreme” biased conditions, e.g. low kurtosis.

## 5. Results

We have applied our method for directing spatial self-organizations, which generates biased initial configurations, to a number of bifurcating shape aggregations. We refer to the resulting shapes as the quarter-moon, ellipse, discs, and two parallel line segments. These shapes (and their associated chemical fields) were utilized in an earlier study [4], and had shown not to produce a single final, aggregated result. In our initial MP work it was not uncommon for the output of the evolution process to generate chemical fields that led to the formation of different shapes from a single field. These four were chosen because they generated two different shapes in equal proportions (except for the parallel lines shape) from uniformly random initial conditions. The chemical field functions that direct MPs to form into these shapes are detailed in Table 1. Given biased initial conditions the aggregation simulations produce one final outcome in almost all of cases. Moreover, by thresholding

Shape	Field Function
quarter-moon	$1.0/(\ln(\ln(\ln(\exp(\sin(\ln(\cos(\theta) * ((d + 0.761214) * \ln(d)) + \ln(d - \theta)))) * (\theta - e^\theta)) - ((\theta - d) * (d/\theta)) - ((\theta - e^\theta) * \ln(\ln(\exp(\sin(\ln(\cos(\theta) * ((d + 0.761214) * \ln(d)) + \ln(d - \theta)))) * (((\theta - e^\theta) - ((\theta - e^\theta) * (d/\theta)) + 0.432846)) - ((\theta - d) * (d/\theta))))))$
ellipse	$1.0/\cos(\theta) + \ln(d)$
discs	$1.0/(\cos(\sin(\theta) - (\cos(\theta) - (\ln(-0.367378)/(\theta + d)))) + \ln(d))$
lines	$1.0/(\ln(\ln(\ln((\cos(\cos(d)) + (d * (3d + \ln(\theta) + \ln(\ln(\theta)))) + ((\ln(\theta)/0.285192) * ((1.0/\theta) + 0.423969))/d)) + d) + d))$

Table 1. The field functions for the MPs utilized in this study. Note that  $\exp(x)$  signifies  $e^x$ .

the moment constraints on the biased initial conditions it is possible to control which shape is produced by a simulation. Figure 4 (top row) shows biased initial conditions for a number of shape aggregations created with this method. The bottom row illustrates the final outcome of each MP simulation that is produced from the associated biased starting configuration.

In order to identify the significant, distinguishing moments for each shape, aggregation simulations (usually several hundred) with unbiased initial conditions are first performed. The shapes of the final outcomes are visually inspected and placed into categories. For each final shape, the mean and standard deviation of the four statistical moments of the evolving system are computed over the entire shape aggregation process. For simulations starting with uniform random, unbiased initial conditions, the final outcomes of the quarter-moon, ellipse and discs shapes evenly split into two categories, with roughly 50% of the final outcomes belonging to each class. The outcomes of the parallel line shapes are unbalanced, with 84.1% belonging to the majority class (two lines) and 15.9% belonging to the minority class (one line). These results, as well as the details that follow in the remainder of the section, are summarized in Table 2.

A typical unbiased aggregation for the quarter-moon shape is shown in Figure 5. The simulation reaches a stable state by 35,000 simulation steps. We identified skewness in the  $x$  coordinate to be the significant macroscopic feature for this shape. See Figure 6 for the evolution of this feature over the course of the aggregation given uniform random initial conditions. Two sets of biased initial conditions (each with 100 examples) were generated with constrained skewness values in the  $x$  coordinate,

Quarter-moon			
Shapes	Unbiased Percentage	Thresholded Moment	Biased Percentage
left-pointing	50%	$Skewness_x \geq 0.315$	100%
right-pointing	50%	$Skewness_x \leq -0.315$	100%
Ellipse			
Shapes	Unbiased Percentage	Thresholded Moment	Biased Percentage
single ellipse	50%	$Kurtosis_y \geq 2.18$	100%
non-single ellipse	50%		0%
two ellipses	–	$Kurtosis_y \leq 1.85$	100%
Multiple Discs			
Shapes	Unbiased Percentage	Thresholded Moment	Biased Percentage
three discs	0%	$Variance_x \leq 10,270$	100%
no three discs	100%	$Variance_x \geq 15,500$	100%
Shapes	Unbiased Percentage	Thresholded Moment	Biased Percentage
three discs	0%		4%
four discs	50%	$1.99 \leq Kurtosis_x \leq 2.09$	75%
five or more discs	50%		21%
Parallel Line Segments			
Shapes	Unbiased Percentage	Thresholded Moment	Biased Percentage
two lines	84.1%	$Kurtosis_x \leq 1.90$	100%
one line	15.9%	$Kurtosis_x \geq 2.29$	100%

Table 2. Table summarizing results generated with unbiased and biased initial conditions.

with the thresholds set as greater than 0.315 (2 standard deviations from the mean) and less than  $-0.315$ . Since the distributions are generated stochastically, they do not have the exact targeted skewness value. So our acceptance test is based on a threshold. We performed simulations with the quarter-moon interaction function for these 200 biased initial conditions. Of the 100 initial conditions with a thresholded third  $x$  moment below  $-0.315$ , 100% of the final outcomes are right-pointing structures. Of the 100 initial conditions with a thresholded third  $x$  moment above 0.315, 100% are left-pointing structures. Figure 7 presents the evolution of this feature over the course of the aggregation given the biased initial conditions.

A typical unbiased aggregation for the ellipse shape is shown in Figure 8, with half of the unbiased initial conditions producing a single “perfect” ellipse, with the other half producing either two ellipses or a deformed “blob”. The unbiased simulation is computed for 10,000 steps. If the simulations are run for 50,000 steps they all will

produce a single ellipse. Kurtosis in the  $y$  direction was found to be the significant macroscopic feature for this shape. See Figure 9 for the evolution of this feature over the course of the aggregation given uniform random initial conditions. 100 simulations were performed with initial conditions that had their  $y$  coordinates' kurtosis thresholded to be above 2.18. Given these biased initial conditions all simulation (100%) produced a perfect single ellipse by step 7,500. 100 additional simulation were performed with initial conditions that had their  $y$  kurtosis set below 1.85. All 100 simulations produced two ellipses by step 7,500. Figure 10 presents the evolution of this feature over the course of the aggregation given the biased initial conditions. These results show that not only can biased initial conditions direct the outcomes of the simulations, but they can also significantly speed up the formation of the desired result, with the single ellipse being guaranteed to form by 50,000 steps in the unbiased case and by 7,500 steps given biased initial conditions.

The discs dataset, when run with 200 unbiased initial conditions, produces 100 four discs structures and 100 structures of five or more discs, with a typical shape aggregation shown in Figure 11. The simulation reaches a stable state by 15,000 steps. We identified variance in the  $x$  direction to be the significant macroscopic feature for this shape. See Figure 12. In our experiments as the variance of the initial conditions was lowered, we found that we could generate a new shape (one that did not appear with unbiased initial conditions), that contained only three discs. Thresholding the  $x$  variance of the initial conditions to be less than 10,270 would always (100%) produce a 3-disc result. A typical 3-disc shape is presented in Figure 4(c). We were unable to consistently generate a 4-disc result for most simulations by thresholding the variance. Thresholding the  $x$  kurtosis to be greater than 1.90 and less than 2.09 did lead to an increased number of 4-disc results (75%), which we deemed as less than consistent or robust. Figure 13 presents the evolution of  $x$  variance over the course of the 3-disc aggregation given the biased initial conditions. Note that no 3-disc results were produced when keeping the  $x$  variance above 15,500 in the biased initial conditions.

The parallel line dataset, when run with unbiased initial conditions, contains 526 instances of two vertical parallel line segments (84.1%) and 100 instances of one vertical line (15.9%), as seen in Figure 14. The simulation reaches a stable state by 50,000 steps. We identified kurtosis in the  $x$  coordinate to be the significant macroscopic feature for the shape. See Figure 15. 100 simulations were performed with initial conditions that had their  $x$  coordinates' kurtosis thresholded to be below 1.90. Given these biased initial conditions all simulation (100%) produced the two line structure. 100 simulations were then performed with initial conditions that had their  $x$  coordinates' kurtosis thresholded to be above 2.29. These biased conditions produced results that consistently (100%) created the minority class structure of a single line by 10,000 steps. Figure 16 presents the evolution of  $x$  kurtosis over the course of the aggregation given the biased initial conditions.

## 6. Discussion

Our experiments show that our agents (MPs) can be reliably directed to form into large-scale, macroscopic structures using local-only behaviors, based on chem-

ical diffusion fields and biased initial conditions; thus producing a stigmergic phenomenon [44]. This type of global outcome is of particular interest to those looking for a robust, adaptable, and independent self-organizing system. A review conducted by the European Space Agency has shown that for their harsh working environment (space, Mars, etc...) the robustness of a local-only system is a key consideration and would allow for relatively simple (and easy to transport) satellites/equipment to form into a larger and more complex system that would be impossible to transport as a monolithic structure [45]. Systems using global information, with centralized communication between primitives, or a command-and-control structure, can form more complex shapes more quickly than local-only approaches. However these systems can fail if this communication is interrupted or the command-and-control structure breaks down [46].

The reasons that certain biased initial conditions may be used to direct the outcome of an aggregation process are frequently visually obvious. For example, the biased initial conditions seen in Figure 4(a) are clearly skewed to the right side of the arena. So it is clear that the majority of the agents are already amassed around the center of the object to be formed. This can also be seen in Figure 4(c), where lowering the variance of the X component makes the initial distribution of the MPs cluster around the central axis which the three discs will form along. The visual evidence that biasing initial conditions effectively pre-starts the aggregation process towards a desired shape is not as evident in the examples that constrain kurtosis ((b) and (d)). A higher Y kurtosis value in example (b) means that there should be a higher concentration of agents along the  $Y = 500$  axis. In (d), a lower X kurtosis value means that there should be more agents distributed away from the center of the arena. But in both of these cases, while statistically this is true, it is not visually evident.

It should be noted that not all shapes are stable throughout the simulation. The vertical lines being a good example; up to approximately 5,000 steps the 1-line and 2-lines shapes look very similar and have similar statistical moments, however between 10,000 and 45,000 steps 15.9% of the simulations will converge into a single line. This shows that some shapes may appear to be stable at one point during a simulation, when actually they have not yet stabilized. Or in other words, our agents may produce more than one type of distinct shape during their evolution. Thus, our experiments show that we are able to consistently produce certain self-organized swarms at a specific point in time during their aggregation.

For these types of self-organizing systems, it is clearly desired to have a completely local solution. Given that the methods described here require the computation of global system-level quantities (moments of the entire distribution) and the manipulation of the locations of the agents in order to meet some global constraint, we have not achieved this goal. In the future, we intend to explore if our genetic programming approach to local chemical field evolution, that leads to the formation of macroscopic shapes, can also be used to find chemical fields (i.e. local interactions) that direct a swarm that is uniformly randomly distributed into one that has specific statistical properties. This would lead to a two-step approach that is truly based on local-only interactions. In this case, the agents, which have been uniformly randomly placed in an environment, would follow chemical fields that move them into a biased initial condition. Then they would switch to a field that

robustly directs them to form in a specific macroscopic shape.

Additional future work with this system will involve robustness testing of the parameters of the initial conditions. Previous work in this area has defined a lower-bound for the number of primitives required to successfully create a single ellipse (400), but has not defined an upper-bound [47]. An upper and lower bound on the number of primitives (which of course is related to MP density) in the simulation is important as more complex shapes are created. Additionally future work will involve further analysis of the aggregation processes that cannot be completely controlled. These investigations should reveal new features that differentiate swarms that can be controlled via the reported method and those that cannot. We imagine that manipulation of other features will further enhance our ability to direct our self-organizing system.

Ultimately we would like to implement our spatial self-organization approach in a swarm robotics system. We believe that this would be feasible with robots that communicate locally via Bluetooth. Given that all robots emit the same field, a single robot can compute the cumulative chemical field and its gradient at its location simply by knowing the distances and angular relationships of neighboring robots from itself. If each robot has a unique broadcasted ID, we imagine that distance could be derived from signal strength and angular information could be computed from inputs from multiple antennae. We have had discussions with a local roboticist about the possibility of using her swarm robotics platform to investigate our methods for distributed control.

## 7. Conclusions

We have previously developed an agent-based self-organizing shape formation system. The agents perform identical behaviors based on sensing local information emitted into the environment by the agents. Genetic programming may be used to discover local interaction rules that lead the agents to self-organize into a number of user-specified shapes. However, since the agents are initially uniformly randomly placed in the environment and they stochastically follow prescribed rules, the aggregation simulations do not always produce the same final results. In order to develop methods that could be used to direct the agents to robustly form one specific configuration, we explored the relationships between an agent swarm's moments and its final configuration. After having shown that these moments could be used to predict the outcome of an MP aggregation in previous work, we demonstrate in this work that biasing the swarm's initial conditions based on these moments can be used to consistently direct the swarm to produce a desired macroscopic shape.

By analyzing the statistical moments of the agents' positions over the entire shape aggregation process, we have identified significant, distinguishing moment features, and utilize them as constraints on simulation initial conditions for a number of bifurcating shapes. Biased initial conditions may be generated that meet these moment constraints, which then affect the resulting shape outcomes. In almost all of our examples we can completely control the result of the self-organization process. In some other cases we can significantly increase the likelihood of producing a desired configuration. In a more general sense, our work also indicates that complex,



non-linear dynamical self-organizing systems may be controlled by manipulating their initial conditions.

### Disclosure/Conflict-of-Interest Statement

The authors declare that the research was conducted in the absence of any commercial or financial relationships that could be construed as a potential conflict of interest.

### Acknowledgments

The authors would like to thank Robert Gilmore, Christian Kuehn and Santiago Ontañón for many helpful discussions and suggestions. This research was funded by National Science Foundation grants CCF-0636323 and IIS-0845415.

### References

- [1] L. Bai, M. Eyiurekli, and D. Breen, *Automated Shape Composition Based on Cell Biology and Distributed Genetic Programming*, in *Proc. Genetic and Evolutionary Computation Conference*, 2008, pp. 1179–1186.
- [2] L. Bai and D. Breen, *Chemotaxis-inspired cellular primitives for self-organizing shape formation*, in *Morphogenetic Engineering: Toward Programmable Complex Systems*, chap. 9, Springer, 2012, pp. 209–237.
- [3] E. Eisenbach, *et al.*, *Chemotaxis*, Imperial College Press, London, 2004.
- [4] L. Bai, R. Gilmore, and D. Breen, *Predicting Spatial Self-Organization with Statistical Moments*, in *Proc. Spatial Computing Workshop of the AAMAS Conference*, 2014, p. Article 2.
- [5] C. Reynolds, *Flocks, herds and schools: A distributed behavioral model*, in *Proc. SIGGRAPH '87*, 1987, pp. 25–34.
- [6] K. Fleischer and A. Barr, *A Simulation Testbed for the Study of Multicellular Development: The Multiple Mechanisms of Morphogenesis*, in *Proc. Artificial Life III*, 1994, pp. 389–408.
- [7] K. Fleischer, *Investigations with a Multicellular Developmental Model*, in *Proc. Artificial Life V*, 1996, pp. 389–408.
- [8] G. Theraulaz and E. Bonabeau, *Coordination in distributed building*, *Nature* 269 (1995), pp. 686–688.
- [9] G. Theraulaz and E. Bonabeau, *Modeling the collective building of complex architectures in social insects with lattice swarms*, *Journal of Theoretical Biology* 177 (1995), pp. 381–400.
- [10] T. Vicsek, A.C. E. Ben-Jacobabd, I. Cohen, and O. Shochet, *Novel type of phase transition in a system of self-driven particles*, *Physical Review Letters* 75 (1995), pp. 1226–1229.
- [11] A. Jadbabaie, J. Lin, and A. Morse, *Coordination of groups of mobile autonomous agents using nearest neighbor rules*, *IEEE Trans. on Automatic Control* 48 (2003), pp. 988–1001.

- [12] P. Eggenberger, *Evolving Morphologies of Simulated 3D Organisms Based on Differential Gene Expression*, in *Proc. 4th European Conference on Artificial Life*, 1997, pp. 205–213.
- [13] P. Hotz, *Combining developmental processes and their physics in an artificial evolutionary system to evolve shapes*, in *On Growth, Form and Computers*, K. S. and P. Bentley, eds., Academic Press, 2003, pp. 302–318.
- [14] E. Bonabeau, S. Guerin, D. Snyers, P. Kuntz, and G. Theraulaz, *Three-dimensional architectures grown by simple ‘stigmergic’ agents*, *BioSystems* 56 (2000), pp. 13–32.
- [15] R. Nagpal, *Programmable self-assembly using biologically-inspired multiagent control*, in *Proc. 1st International Joint Conference on Autonomous Agents and Multiagent Systems: part 1*, 2002, pp. 418–425.
- [16] R. Nagpal, A. Kondacs, and C. Chang, *Programming Methodology for Biologically-Inspired Self-Assembling Systems*, in *Proc. AAAI Spring Symposium on Computational Synthesis*, 2003, pp. 173–180.
- [17] K. Stoy and R. Nagpal, *Self-reconfiguration using directed growth*, in *Proc. Internatioanl Symposium on Distributed Autonomous Robotic Systems*, 2004, pp. 3–12.
- [18] E. Rimon and D. Koditschek, *Exact robot navigation using artificial potential functions*, *IEEE Trans. on Robotics and Automation* 8 (1992), pp. 501–518.
- [19] M. Hsieh and V. Kumar, *Pattern generation with multiple robots*, in *Proc. IEEE International Conference on Robotics and Automation*, Orlando, Florida, 2006, pp. 2442–2447.
- [20] W.M. Shen, P. Will, A. Galstyan, and C.M. Chuong, *Hormone-inspired self-organization and distributed control of robotic swarms*, *Autonomous Robots* 17 (2004), pp. 93–105.
- [21] H. Sayama, *Swarm chemistry*, *Artificial Life* 15 (2009), pp. 105–114.
- [22] H. Sayama, *Robust morphogenesis of robotic swarms*, *IEEE Computational Intelligence* 5 (2010), pp. 43–49.
- [23] K. Sims, *Interactive Evolution of Dynamical Systems*, in *Proc. 1st European Conference on Artificial Life*, 1992, pp. 171–178.
- [24] M. Mamei, M. Vasirani, and F. Zambonelli, *Experiments of morphogenesis in swarms of simple mobile robots*, *Applied Artificial Intelligence* 18 (2004), pp. 903–919.
- [25] S. Von Mammen and C. Jacob, *The evolution of swarm grammars-growing trees, crafting art, and bottom-up design*, *IEEE Computational Intelligence Magazine* 4 (2009), pp. 10–19.
- [26] M. Prokopenko (ed.), *Guided Self-Organization: Inception*, Springer, Berlin, 2014.
- [27] R. Doursat, *The growing canvas of biological development: Multiscale pattern generation on an expanding lattice of gene regulatory nets*, in *Unifying Themes in Complex Systems*, Springer Verlag, 2008, pp. 205–210.
- [28] R. Doursat, *Organically grown architectures: Creating decentralized, autonomous systems by embryomorphic engineering*, in *Organic Computing*, R. Würtz, ed., chap. 8, Springer Verlag, 2008, pp. 167–200.
- [29] J. Werfel, K. Petersen, and R. Nagpal, *Designing collective behavior in a termite-inspired robot construction team*, *Science* 343 (2014), pp. 754–758.

## REFERENCES

19

- [30] V. Gerling and S. Von Mammen, *Robotics for Self-Organised Construction*, in *Foundations and Applications of Self\* Systems, IEEE International Workshop on*, 2016, pp. 162–167.
- [31] R. Pfeifer, M. Lungarella, and F. Iida, *Self-organization, embodiment, and biologically inspired robotics*, *Science* 318 (2007), pp. 1088–1093.
- [32] L. Bai, M. Eyiuyurekli, P. Lelkes, and D. Breen, *Self-organized sorting of heterotypic agents via a chemotaxis paradigm*, *Science of Computer Programming* 78 (2013), pp. 594–611.
- [33] S. Gilbert, *Developmental Biology*, 10th ed., Sinauer Associates, Inc., Sunderland, MA, 2013.
- [34] J. Davies, *Mechanisms of Morphogenesis: The Creation of Biological Form*, Elsevier, Amsterdam, 2005.
- [35] M. Eyiuyurekli, P. Manley, P. Lelkes, and D. Breen, *A computational model of chemotaxis-based cell aggregation*, *BioSystems* 93 (2008), pp. 226–239.
- [36] T. Sekimura, S. Noji, N. Ueno, and P. Maini (eds.), *Morphogenesis and Pattern Formation in Biological Systems*, Springer, Tokyo, 2003.
- [37] J. Koza, *Genetic Programming: On the Programming of Computers by Means of Natural Selection*, MIT Press, Cambridge, MA, 1992.
- [38] L. Bai, *Self-Organizing Primitives for Automated 2D Shape Composition*, , Master’s thesis, Drexel University, Philadelphia, PA (2008).
- [39] L. Bai, *Chemotaxis-based Spatial Self-Organization Algorithms*, Ph.D. thesis, Drexel University, Philadelphia, PA, 2014.
- [40] S. Wiggins (ed.), *Introduction to Applied Nonlinear Dynamical Systems and Chaos, 2nd Edition*, Springer, New York, 2003.
- [41] N. Cristianini and J. Shawe-Taylor, *An Introduction to Support Vector Machines and Other Kernel-Based Learning Methods*, Cambridge University Press, 2000.
- [42] S. Seabold and J. Perktold, *Statsmodels: econometric and statistical modeling with python*, in *Proc. 9th Python in Science Conference*, 2010, pp. 57–61.
- [43] R.M. Neal, *Slice sampling*, *Annals of Statistics* (2003), pp. 705–741.
- [44] G. Theraulaz and E. Bonabeau, *A brief history of stigmergy*, *Artificial Life* 5 (1999), pp. 97–116.
- [45] *Swarm intelligence* (2017), Retrieved October 23, 2017, <http://www.esa.int/gsp/ACT/ai/projects/swarm.html>.
- [46] L. Pettazzi, D. Izzo, and S. Theil, *Swarm navigation and reconfiguration using electrostatic forces*, in *Proc. 7th International Conference On Dynamics and Control of Systems and Structures in Space*, 2006, pp. 257–268.
- [47] L. Bai, M. Eyiuyurekli, and D. Breen, *An Emergent System for Self-Aligning and Self-Organizing Shape Primitives*, in *Proc. IEEE International Conference on Self-Adaptive and Self-Organizing Systems Conference*, 2008, pp. 445–454.

Figures



Figure 1. Morphogenetic Primitives self-organizing into a star shape. Initially published in [2].

REFERENCES

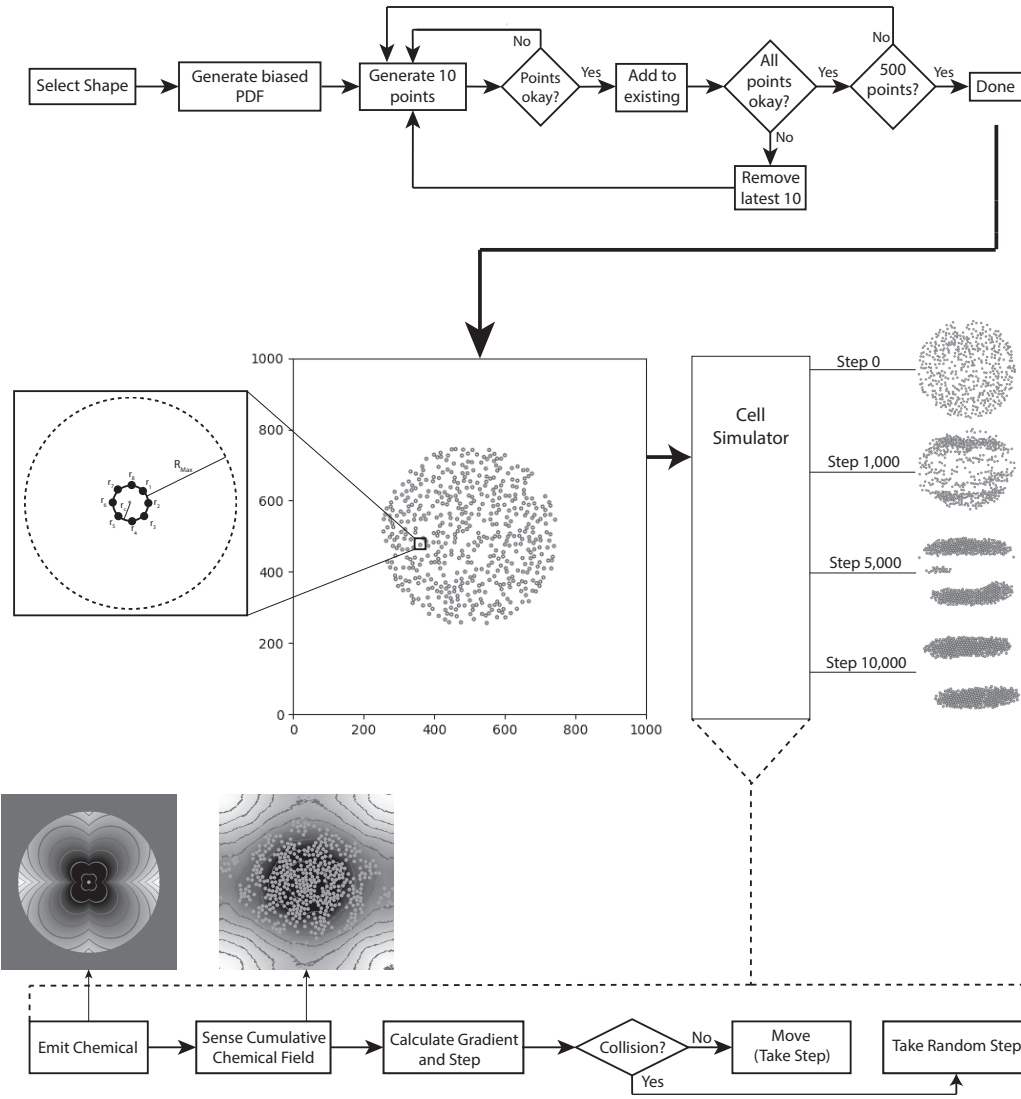


Figure 2. Schematic diagram of the directed self-organization process based on specifying biased initial conditions for Morphogenetic Primitives.

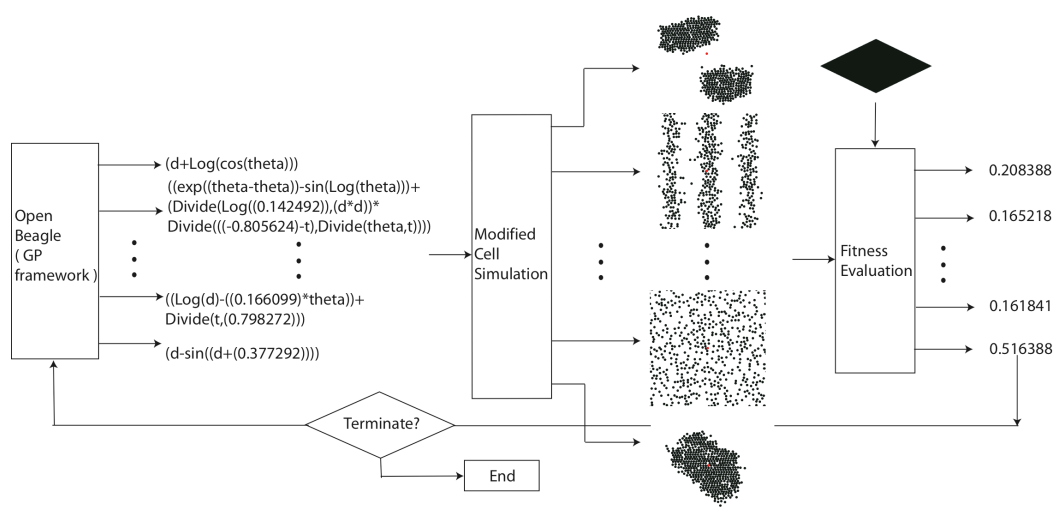


Figure 3. The genetic programming process that produces the local chemical field functions of the shape primitives. Initially published in [1].

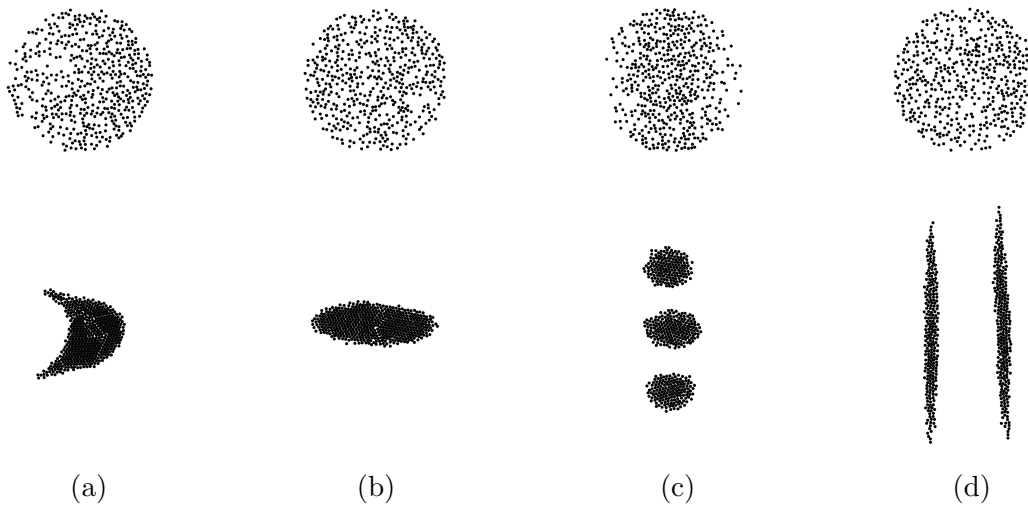


Figure 4. (top row) Biased initial conditions ((a)  $x$  skewness = -0.315, (b)  $y$  kurtosis = 2.150, (c)  $x$  variance = 9,596, (d)  $x$  kurtosis = 1.88) that robustly evolve (bottom row) into (a) a right-pointing quarter-moon, (b) a single ellipse, (c) three discs and (d) two line segments.

REFERENCES

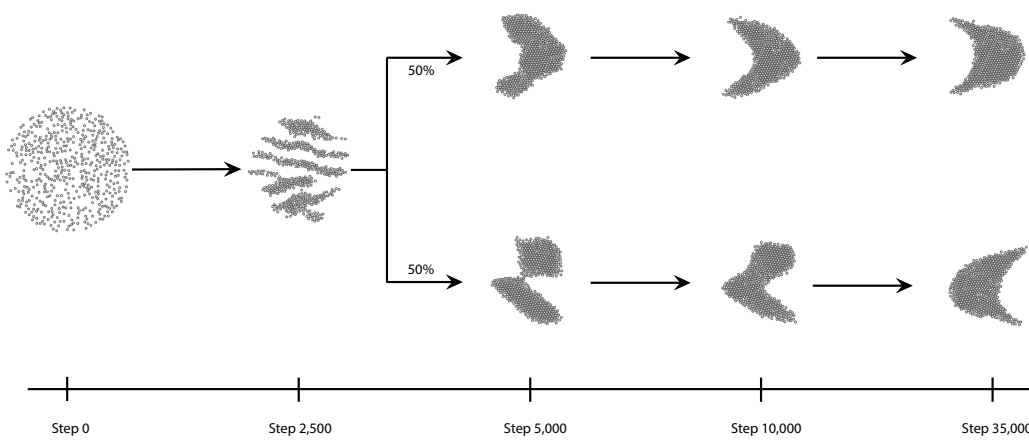


Figure 5. Shape aggregation of the quarter-moon MPs starting from random initial conditions.



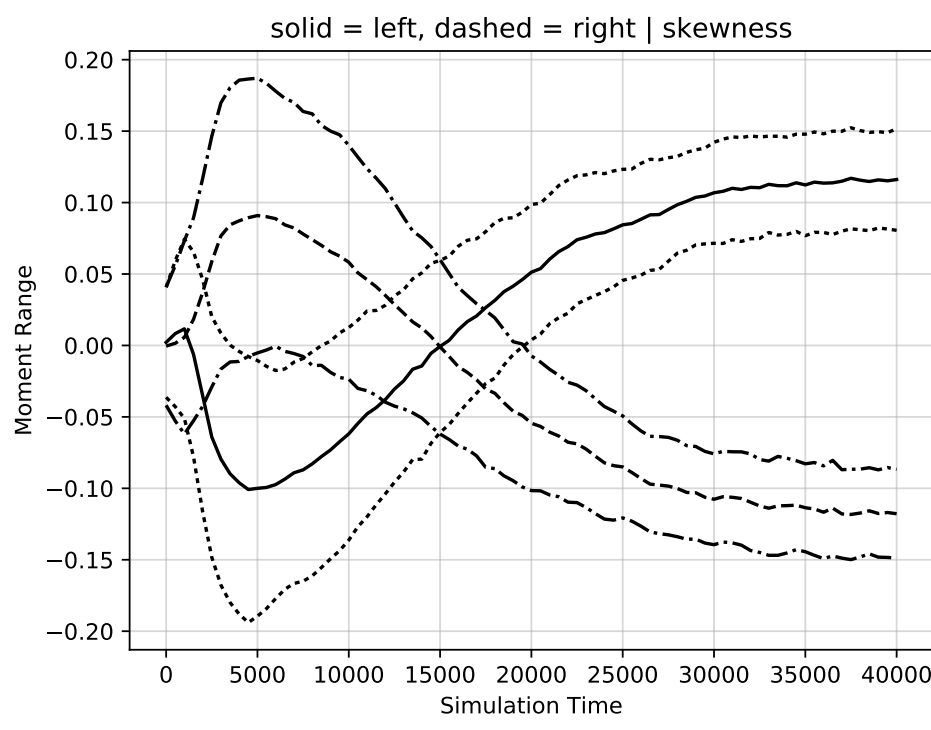


Figure 6. Skewness of the  $x$  coordinate of the unbiased quarter-moon shape aggregations over time.

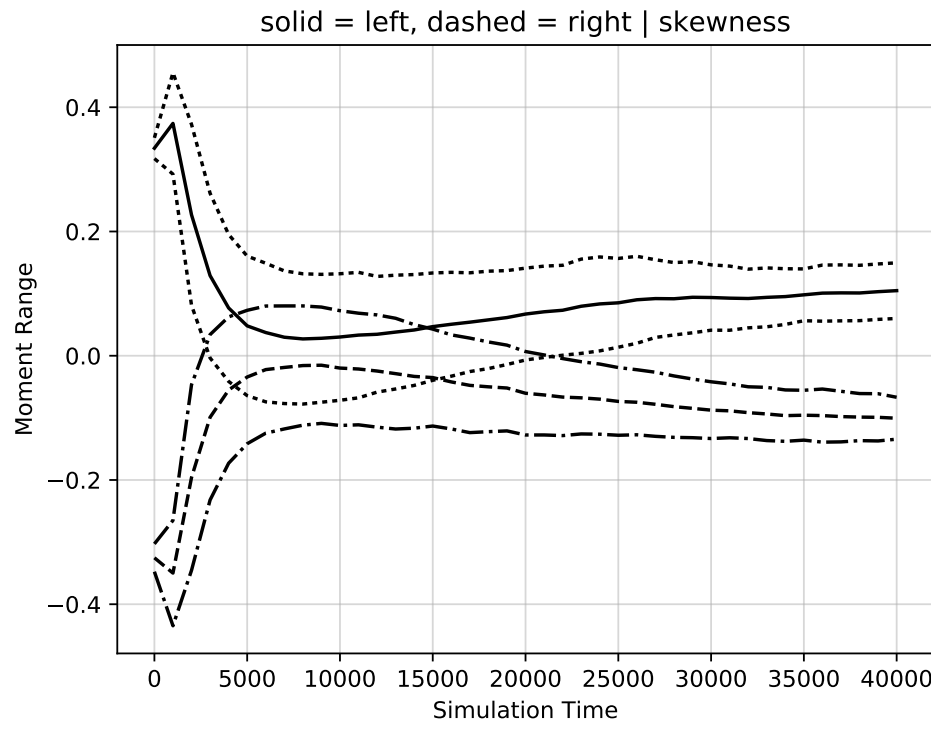


Figure 7. Skewness of the  $x$  coordinate of the biased quarter-moon shape aggregations over time.

REFERENCES

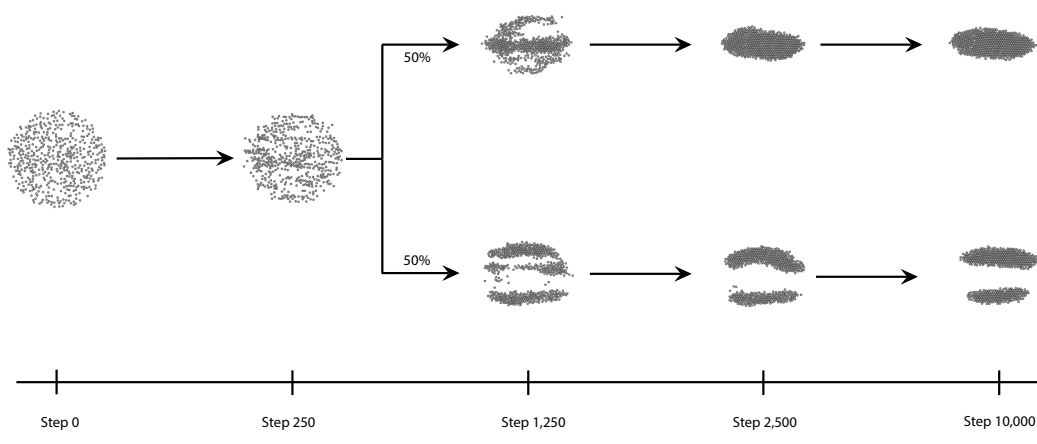


Figure 8. Shape aggregation of the ellipse MPs starting from random initial conditions.

REFERENCES

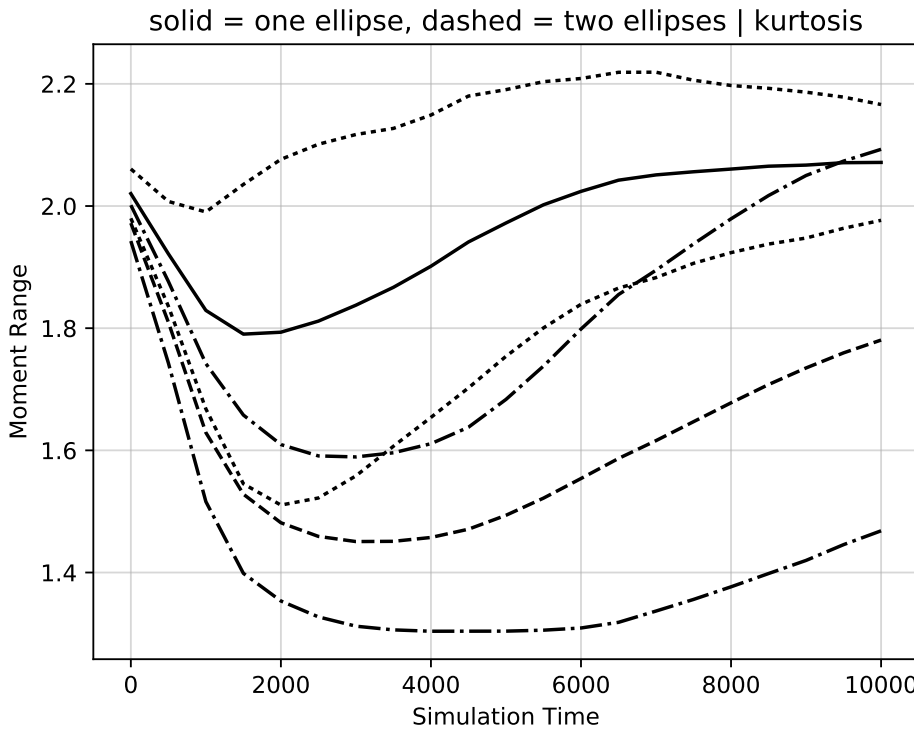


Figure 9. Kurtosis of the  $y$  coordinate of the unbiased ellipse shape aggregations over time.

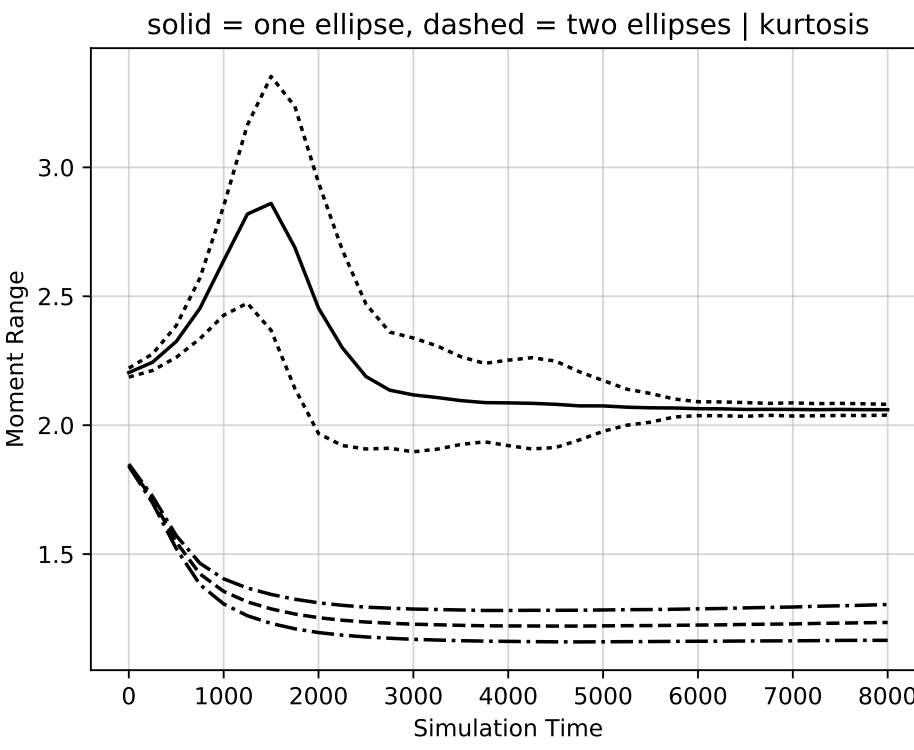


Figure 10. Kurtosis of the  $y$  coordinate of the biased ellipse shape aggregations over time.

REFERENCES

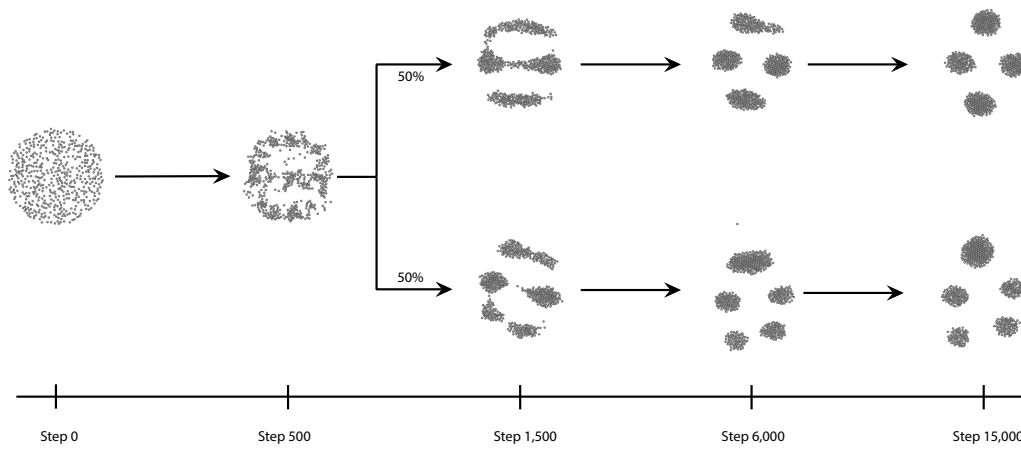


Figure 11. Shape aggregation of the discs MP starting with random initial conditions.

REFERENCES

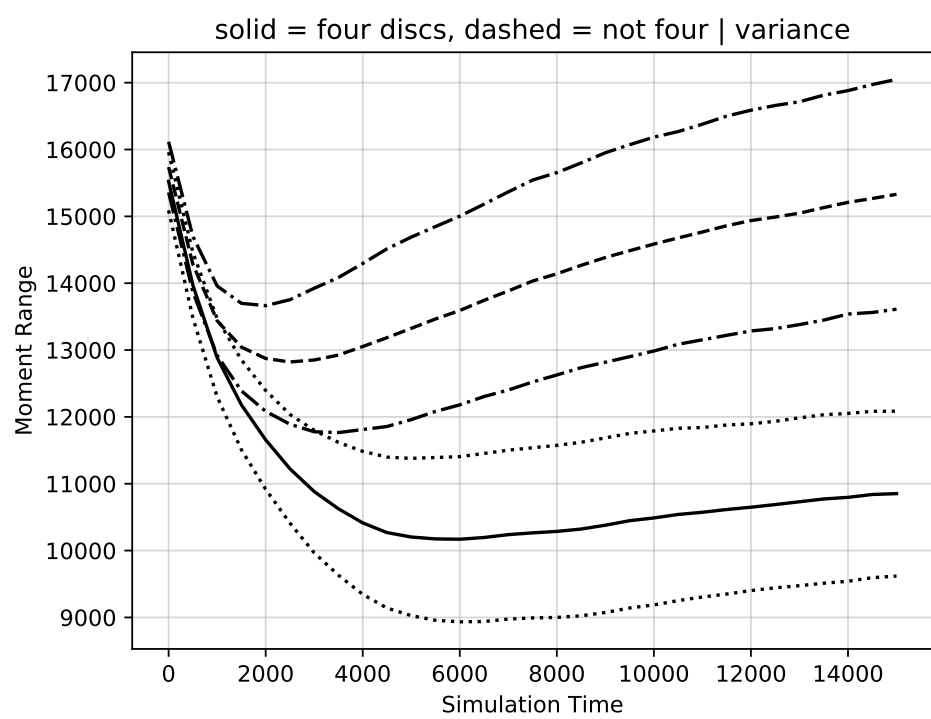


Figure 12. Variance of the  $x$  coordinate of the unbiased discs shape aggregations over time.

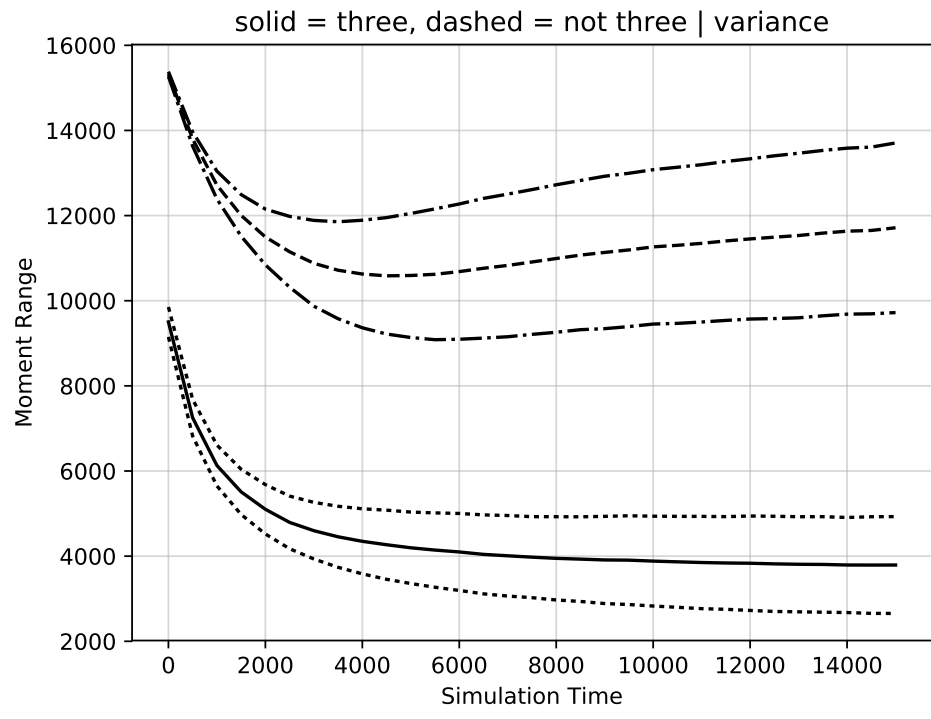


Figure 13. Variance of the  $x$  coordinate of the biased discs shape aggregations over time.

REFERENCES

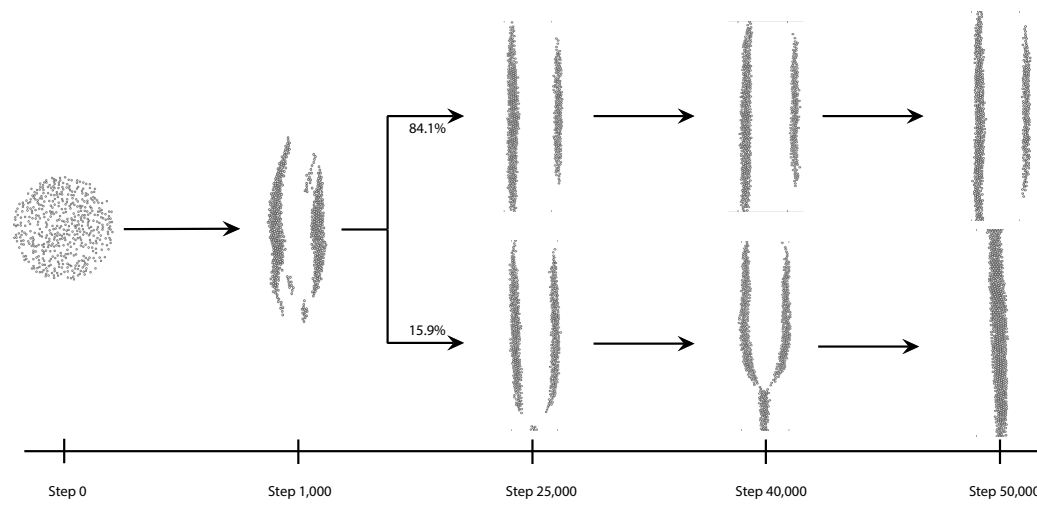


Figure 14. Shape aggregation of the line segment MPs starting from random initial conditions.

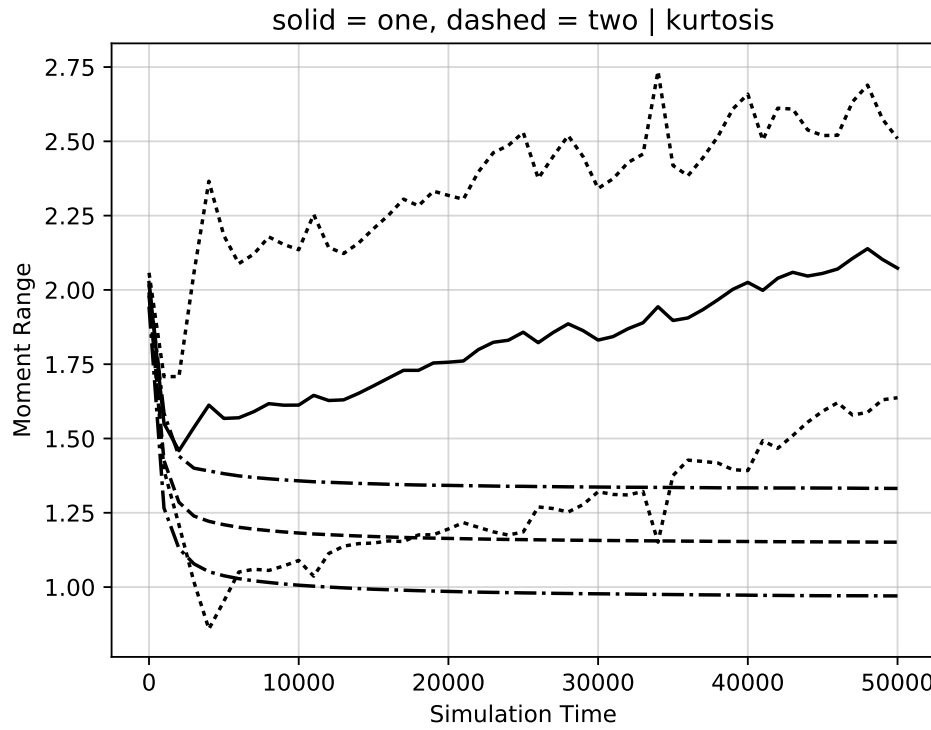


Figure 15. Kurtosis of the  $x$  coordinate of the unbiased line segment shape aggregations over time.

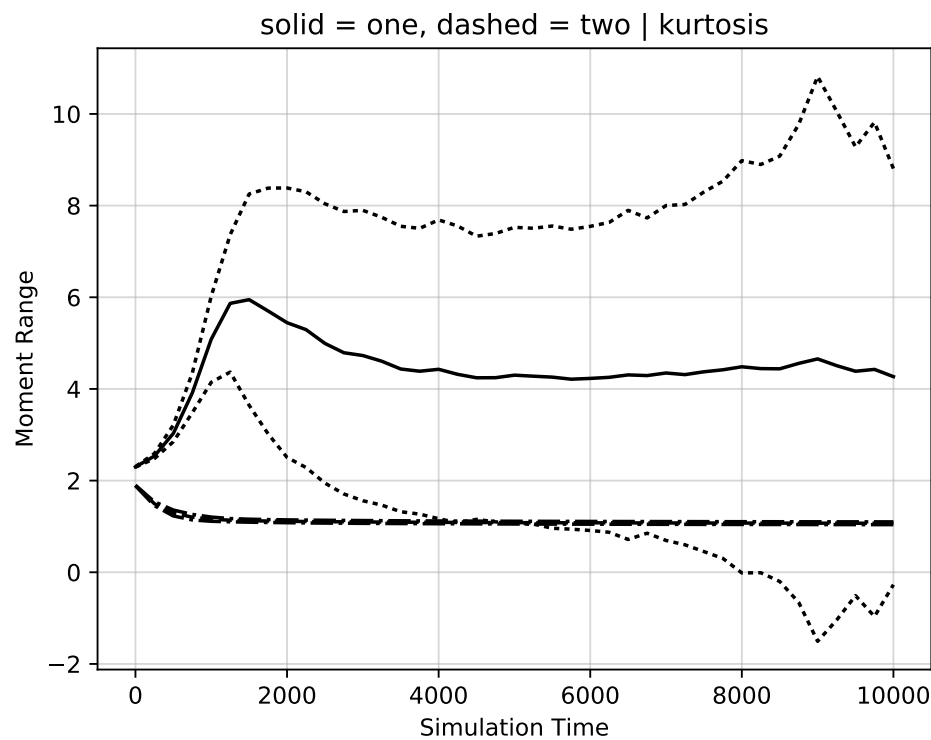


Figure 16. Kurtosis of the  $x$  coordinate of the biased line segment shape aggregations over time.